

FREQUENCY-BASED SIGNAL PROCESSING FOR ULTRASOUND COLOR FLOW IMAGING

Alfred C.H. Yu, K. Wayne Johnston, and Richard S.C. Cobbold

Institute of Biomaterials and Biomedical Engineering, University of Toronto
164 College Street, Toronto, ON, Canada. M5S 3G9
cobbold@ecf.utoronto.ca

ABSTRACT

In ultrasound color flow imaging, the computation of flow estimates is well-recognized as a challenging problem from a signal processing perspective. The flow visualization performance of this imaging tool is often affected by error sources such as the lack of abundant signal samples available for processing, the presence of wideband clutter in the acquired signals, and the flow signal distortions that may arise during clutter suppression. In this article, we review existing frequency-based signal processing approaches reported in the ultrasound literature and evaluate their theoretical advantages as well as limitations. In particular, four major classes of clutter filter designs are considered: FIR/IIR filtering, polynomial regression, clutter-downmixing, and eigen-regression. Also, three types of frequency estimators are discussed: lag-one autocorrelation, autoregressive modeling, and MUSIC. In examining these approaches, it was concluded that eigen-based methods like the eigen-regression filter and the MUSIC estimator can better adapt to the Doppler signal characteristics, and thus they seem to have more potential for obtaining flow estimates that are less affected by the signal processing error sources.

SOMMAIRE

En imagerie couleur en flux d'ultrasons, le calcul des estimations d'écoulement est un problème bien connu d'un point de vue traitement de signaux. La performance de cet outil d'imagerie au niveau de la visualisation, est souvent affectée par différentes sources d'erreur telles que le manque de signaux disponibles par échantillon pour le traitement, la présence de clutter à bande large durant l'acquisition, et les déformations de signal d'écoulement qui peuvent surgir pendant la suppression des clutter à bandes larges. Dans cet article, nous passons en revue les approches actuelles décrites dans la littérature de traitements de signaux basées sur la fréquence, et nous évaluons leurs avantages théoriques ainsi que leur limitations. En particulier, les principales classes de conceptions de filtre de clutter considérées incluent: la filtration FIR/IIR, la régression polynomiale, le bas-mélange de clutter, et l'eigen-régression. Trois types d'estimateurs de fréquence sont discutés, à savoir, l'autocorrélation lag-one, la modélisation auto-régressif, et MUSIC. En examinant ces approches, nous avons pu conclure que les méthodes basées sur eigen- tel que le filtre de régression eigen et l'estimateur de MUSIC peuvent mieux s'adapter aux caractéristiques de signal de Doppler. Par conséquent, les stratégies de traitement de signaux basées sur eigen semblent être plus aptes à obtenir des estimations d'écoulement qui sont moins affectées par les sources d'erreur de traitement de signaux.

1. INTRODUCTION

Ultrasound color flow imaging is a diagnostic tool that is useful to the study of cardiovascular flow dynamics. As reviewed by Ferrara and DeAngelis [1], it has been used to identify the presence of vascular stenoses, assess complicated flow patterns, diagnose for the development of aneurysms and tumors, study the patency of implanted shunts, and visualize blood regurgitations between heart chambers during a cardiac cycle. More recently, this diagnostic tool has found new applications such as micro-circulation assessment in the eyes [2], treatment response monitoring during cancer therapies [3], contractility exam-

ination of heart muscles [4], and guidance of interventional devices [5]. Comparing with other non-invasive vascular imaging modalities such as magnetic resonance angiography, ultrasound color flow imaging has the advantage of being able to provide flow information in real-time [6]. Further-more, it is an imaging tool that is more affordable by most clinics.

Given the widespread use of ultrasound color flow imaging in medical diagnostics, it is important for these images to provide accurate visualization of the vascular flow dynamics. As pointed out in some evaluation studies (e.g. see [7][8]), failure to provide accurate flow information in color flow images may lead to an increased risk of mis-

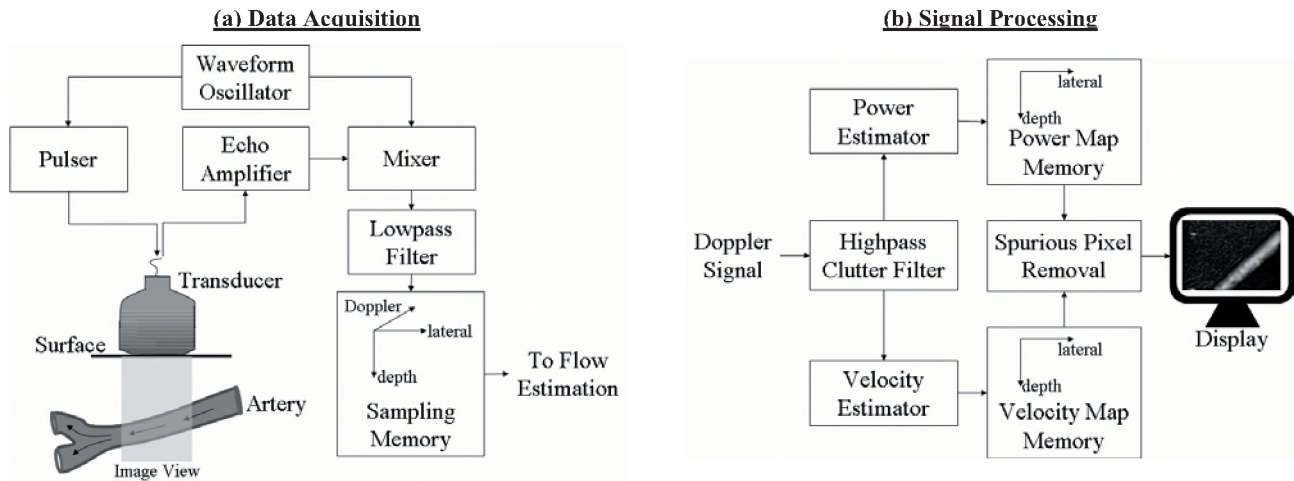


Figure 1. Overview of a generic ultrasound color flow imaging system. Shown in (a) and (b) are the block diagrams for the data acquisition and signal processing stages.

diagnosis and may cause assessment difficulties during long-term patient monitoring. However, from a signal processing perspective, there are several factors that tend to reduce the accuracy of blood flow estimates displayed in color flow images. These sources of errors can generally be divided into two categories: 1) those that arise during suppression of clutter in the color flow data, and 2) those that arise during estimation of blood flow velocities. The main signal processing sources of errors encountered during clutter suppression are mainly associated with the small Doppler ensemble size (less than 20 samples) available for data processing and the possible presence of wideband clutter when using longer data acquisition periods. On the other hand, the primary signal processing error source in velocity estimation is related to the blood signal distortions resulting from the clutter filtering process. In terms of their impact, these error sources may lead to the appearance of spurious or erroneous flow map pixels (commonly referred to as flash artifacts) in the color flow images. In turn, they may obscure visualization of the underlying flow dynamics.

The intent of this paper is to point out the origin of signal processing problems encountered in ultrasound color flow imaging and survey the approaches that have been reported previously to resolve these problems. In particular, it is our intent to theoretically compare various clutter filter designs and frequency-based flow estimation methods reported in the ultrasound literature. To help formulate our discussion, we begin with a general overview on the principles of color flow imaging. The signal processing error sources and existing solutions will then be described later on. Note that many of the signal processing strategies covered in this article are also used in advanced color flow imaging schemes like three-dimensional (3D) flow mapping [9], dual-beam vector flow studies [10], high-frequency flow imaging [11], and contrast-enhanced flow studies [12]. However, this article will not directly discuss the issues specific to these advanced imaging techniques.

2. OVERVIEW OF ULTRASOUND COLOR FLOW IMAGING

2.1. Fundamental Principles

As recently pointed out in a historical account by Cobbold [13] (Sec. 10.7), ultrasound color flow imaging was first commercially introduced in the 1980s. This technique is based on the periodic transmission of finite-duration ultrasound pulses into the imaging view and the subsequent processing of pulse echoes returned from tissue as well as blood scatterers. For this technique, flow information is derived by measuring the relative time shifts between pulse echoes (i.e. pulse-to-pulse changes in the echo return time), whereby the shift magnitude is dependent on the scatterer velocity. As derived in various ultrasound textbooks (e.g. see Sec. 10.2 in [13]), the inter-pulse time shift t_D can be described by the following expression:

$$t_D = \frac{2vT_{PRI}}{c_o} \cos \theta, \quad (1a)$$

where v is the scatterer velocity, T_{PRI} is the pulse repetition interval, c_o is the speed of sound, θ is the beam-flow angle, and the factor of two indicates round-trip propagation. Note that the time shifts described in (1a) can actually be interpreted as a frequency-shift mechanism. In particular, given that frequency is equal to the phase change over time (by definition), the time shift between pulse echoes carries the following frequency interpretation:

$$f_D = \frac{\Delta\phi}{\Delta t} \approx \frac{f_o t_D}{T_{PRI}} = \frac{2vf_o}{c_o} \cos \theta, \quad (1b)$$

where $\Delta\phi = f_o t_D$ indicates the phase change between pulse echoes. It is worth pointing out that (1b) essentially has the same form as the Doppler equation that is well-known in physics. Hence, color flow imaging is often perceived as a Doppler-based flow visualization technique.

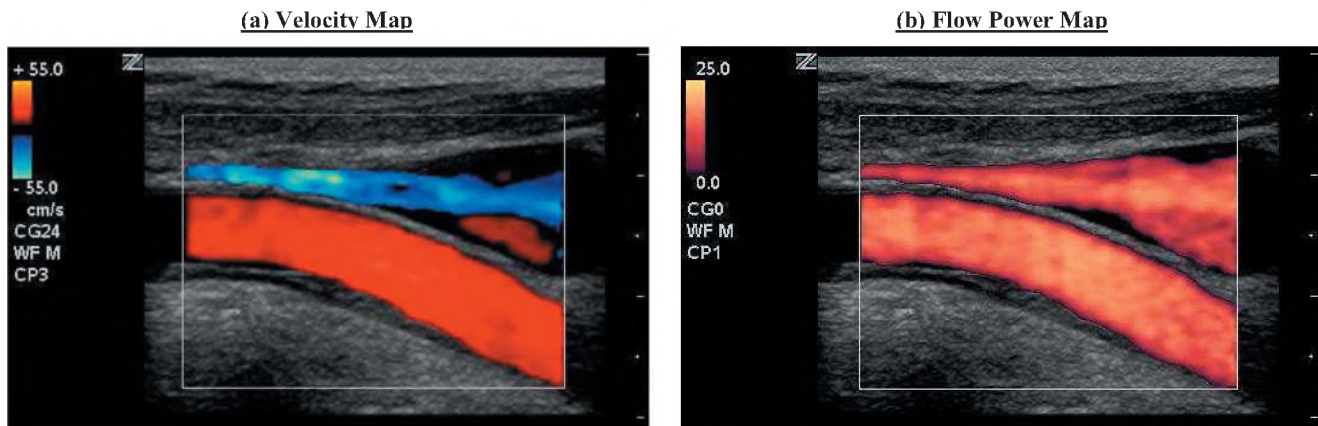


Figure 2. Color flow images for an in-plane slice of a human common carotid artery and jugular vein. (a) Velocity map showing directional flow in red and blue hues; (b) Flow power map showing blood signal strength in pale-red hues. Reproduced with permission from ZONARE Medical Systems (Mountain View, CA, USA).

2.2. System-Level Description

Data Acquisition

From a system-level perspective, the formation of each color flow image can be divided into two main stages: data acquisition and signal processing. As illustrated in Figure 1a, the data acquisition stage first involves the use of an ultrasound transducer (often an array transducer) to transmit the pulse firings and collect the returned echoes. In order to produce an image, the pulse firing sequence is repeated for different beam lines within the field of view. Subsequently, the received echoes from the different pulse firings are individually downmixed to baseband by mixing the echoes with the carrier frequency of the transmitted pulse and applying a lowpass filter to retain only the baseband spectral components in the mixed echoes. For this downmixing process, the in-phase/quadrature (I/Q) demodulation scheme is often implemented so that the analytic form of the pulse echoes can be obtained for subsequent analysis. After the pulse echoes are downmixed, they are sampled at time points that correspond to various depths in order to study the inter-pulse phase changes or time shifts at various axial and lateral positions (i.e. sample volumes) within the field of view. The resulting data samples can then be arranged into a 3D data array: one dimension for pulse number, one for depth/axial position, and the other for line/lateral position. Since the pulse-number dimension of the 3D data array essentially contains information on the inter-pulse phase changes, this dimension is also referred to as the Doppler axis¹. As well, the ensemble of pulse echo samples for a particular sample volume is referred to as the Doppler signal. Note that, in general, this entire data acquisition procedure can be considered as a sampling mechanism in which one Doppler data sample is collected for each sample volume along a beam line during each pulse firing.

¹ The pulse-number dimension is also referred to as the “slow-time” axis, while the depth dimension is sometimes called the “fast-time” axis.

Signal Processing

In the signal processing stage of ultrasound color flow imaging, a flow power map and a velocity map are computed from the array of Doppler signals acquired through the pulse firings. Most commercial systems compute these two forms of flow information through a frequency-based estimation approach (i.e. by studying the inter-pulse phase changes) because of its relatively simpler computation complexity as compared to time-shift-based estimation approaches (see Sec. 4.5.3 in [14]). As shown in Figure 1b, the frequency-domain flow estimation process first involves the use of a digital highpass filter to suppress low-frequency echoes that may be present in each Doppler signal. This filtering operation is carried out in attempt to distinguish the Doppler echoes of blood scatterers from signal clutter originating from acoustic reverberations of nearby tissues (whose strength can reach 60-80 dB greater than blood depending on the scanner’s dynamic range). After the filtered data samples are obtained, the average power of each post-filter Doppler signal is estimated by simply finding the mean-squared signal value. The velocity estimate for each sample volume is also determined by first finding the mean Doppler frequency of the filtered signal and then converting this estimate into a velocity value via the Doppler equation (and assuming that the other parameters are constants). Once the power and velocity estimates are computed for all the sample volumes, they are turned into image pixels by respectively mapping the flow estimates onto a power map color scale and a velocity map color scale. Since blood flow may not be present in all places within the field of view, spurious map pixels are removed from the power and velocity maps if their corresponding filtered Doppler power is below a threshold. Finally, the resulting flow map is superimposed onto a B-mode image to form a duplex display, thereby enabling the flow information to be related to the underlying structure.

Figure 2 shows an example of flow power map and velocity map for a human common carotid artery and the adjacent jugular vein. Note that, at large beam-flow angles, the flow power map has diagnostic advantage over the

velocity map because the echo power returned from blood scatterers is essentially independent of the beam-flow angle (while the time shift magnitude is angle-dependent). On the other hand, the velocity map has the advantage of being able to provide directional flow information that is clinically important for the identification of arteries and veins.

3. SIGNAL PROCESSING CHALLENGES IN COLOR FLOW IMAGING

3.1. Challenges in Clutter Suppression

Doppler Ensemble Size Limitations

In color flow imaging, the range of pulse repetition intervals that can be used for data acquisition is bounded by two factors: real-time imaging requirements and imaging depth limits. In particular, the maximum pulse repetition interval mainly depends on real-time constraints because all the pulse echoes from every beam line need to be acquired within a frame period that corresponds to a real-time frame rate (i.e. at least 5-10 Hz). On the contrary, the minimum pulse repetition interval depends primarily on the maximum imaging depth because sufficient time between firings is needed to collect pulse echoes from the field of view. Based on the two constraints, the pulse repetition interval T_{PRI} must be defined within the following range for a given maximum depth d_{max} , acoustic speed c_o , frame period T_F , number of beam lines N_L , and Doppler ensemble size N_D :

$$\frac{2d_{max}}{c_o} \leq T_{PRI} \leq \frac{T_F}{N_L N_D}. \quad (2)$$

Amongst the three dependent factors seen in the upper limit of (2), the Doppler ensemble size N_D is the only factor that can be modified for a given image dimension and frame rate. Typically, for an imaging view with 30-60 beam lines, the ensemble size available for each Doppler sample volume is limited to fewer than 20 samples so that the pulse repetition interval can be set to a value that satisfies both real-time constraints and imaging depth limits. However, with such a small ensemble size, it becomes more difficult to suppress low-frequency clutter in the Doppler signal because the transient response of digital filters tends to dominate the filter output for small input ensembles [15]. In order to address this problem, it is necessary to develop strategies that can mitigate the transient filtering effects.

Wideband Clutter Problems

Since the Doppler ensembles are sampled data after all, they are inherently limited to a finite Doppler spectral resolution. From sampling theory, it is well-known that the spectral resolution inversely depends on the ensemble period (i.e. $f_{D(res)} = 1/N_D T_{PRI}$). By substituting this relation into the Doppler equation as given by (1b), the velocity resolution of a Doppler ensemble is given by:

$$v_{res} = \frac{c_o}{2f_o N_D T_{PRI} \cos \theta}. \quad (3)$$

As seen in (3), an increase in ensemble period $N_D T_{PRI}$ or ultrasound frequency f_o can result in an improved velocity

resolution, which is often important for studying slow flow dynamics. However, amongst these two factors, it is only feasible to increase the ensemble period when imaging low-velocity flow at greater depths because high-frequency ultrasound cannot penetrate well into tissue. Such a lengthening of the ensemble period though may be a problem because tissues may undergo substantial motion over this extended period. As pointed out by Heimdal and Torp [16], the clutter component of the Doppler signal may become more wideband as a result and may actually be shifted away from zero frequency. To account for this wideband Doppler clutter, it may be possible to simply use a highpass filter that has a widened stopband (plus suitable transient-reduction methods). Nonetheless, this approach may concomitantly suppress a substantial portion of the blood echoes.

3.2. Challenges in Velocity Estimation

Carrier Frequency Variations

Given the filtered Doppler signal, one simple way of estimating the mean flow velocity is to compute the mean Doppler frequency from the Doppler spectral moments and then use (1b) to convert the mean frequency estimate into velocity. However, the resulting velocity estimates may be biased when there are variations in the carrier frequency of returned echoes simply because the pulse carrier frequency is one of the governing factors in the Doppler equation [17]. As described in a few studies [18][19], attenuation and scattering are the two primary distortion mechanisms that affect the pulse carrier frequency. They tend to bring about a gradual shift in the pulse carrier frequency as the imaging depth increases, and the shift magnitude per unit depth is mainly dependent on the bandwidth of the transmit pulse. Fortunately, this problem is usually of less concern in color flow imaging because narrowband transmit pulses (in the form of multi-cycle sinusoidal bursts) typically need to be used in order to improve the blood echo sensitivity and maintain adequate blood-signal-to-noise ratios. Nonetheless, variations in the carrier frequency can become a significant velocity biasing problem when wideband transmit pulses are used for data acquisition.

Clutter Filter Distortions

The primary side effect of using a filter to suppress low-frequency clutter is that the blood component of the Doppler signal may be distorted due to non-idealities in the filter's frequency response [20][21]. The distortions can be particularly severe if the blood signal's Doppler spectral components are located near the cutoff frequency and its transition region. As a result of these potential distortions, there may be a bias in the mean velocity estimates computed from the filtered Doppler signal. Note that, at low blood-signal-to-noise ratios, the biasing problem becomes worse because the clutter filter also distorts the background white noise and thereby adds further bias to the flow estimates. Hence, the clutter filter is often considered as a principal source of bias in the velocity estimation process.

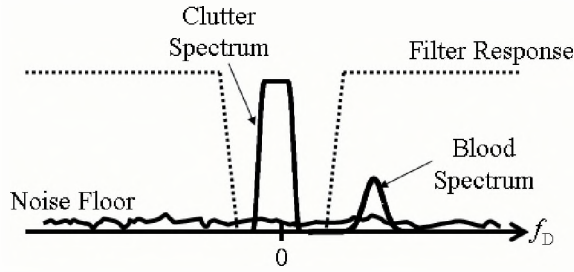


Figure 3. Illustration of the typical spectral contents in a Doppler signal (before digital sampling). Prior to flow estimation, it is often necessary to suppress the high-energy, low-frequency clutter in the Doppler signal.

To avoid this biasing source, it is beneficial to develop velocity estimation methods that can be directly applied to the raw (i.e. unfiltered) Doppler data.

4. EXISTING CLUTTER FILTER DESIGNS

4.1. Non-Adaptive Filters

Background Considerations

To facilitate description of clutter filter designs, we first consider a simple Doppler signal model for an individual sample volume (or map pixel location). As shown in Figure 3, the Doppler signal is consisted of low-frequency clutter echoes, blood echoes, and random white noise. For a given Doppler ensemble size N_D , this signal model can be written in the following vector form:

$$\mathbf{x} = [x(0), x(1), \dots, x(N_D - 1)]^T = \mathbf{b} + \mathbf{c} + \mathbf{w}, \quad (4)$$

where $x(n)$ is the n^{th} Doppler data sample, while \mathbf{x} , \mathbf{b} , \mathbf{c} , and \mathbf{w} are vectors of length N_D for the Doppler signal, the blood echoes, the clutter echoes, and white noise respectively. To study the Doppler frequency (or time shifts) of blood echoes in the Doppler signal, it is often necessary to first use a highpass filter to suppress the high-energy, low-frequency clutter. From a vector space perspective, this filtering task can be considered as the application of a linear matrix operator on the Doppler signal vector. As such, the filtered Doppler signal vector \mathbf{y} can be expressed as follows:

$$\mathbf{y} = [y(0), y(1), \dots, y(N_D - 1)]^T = \mathbf{F}\mathbf{x}, \quad (5)$$

where $y(n)$ is the n^{th} filtered sample and \mathbf{F} is an $N_D \times N_D$ filter matrix. Note that, depending on how the filter matrix is formed, the clutter filter may have a time-variant frequency response. Thus, as pointed out by Torp [15], the filter's frequency response may not be equal to the Fourier transform of its impulse response. Nevertheless, it is still possible to numerically compute the frequency response of these time-variant clutter filters by finding the filter's output power for different complex sinusoid inputs. Based on this notion, the filter response $H(f_D)$ at a particular Doppler frequency can be expressed as follows:

$$H(f_D) = \|\mathbf{F}\mathbf{v}_{CS}\|^2 = \mathbf{v}_{CS}^H \mathbf{F}^H \mathbf{F} \mathbf{v}_{CS}, \quad (6a)$$

where \mathbf{v}_{CS} is a complex sinusoid vector of length N_D , and is given by:

$$\mathbf{v}_{CS} = [1, e^{j2\pi f_D}, \dots, e^{j2\pi f_D(N_D-2)}, e^{j2\pi f_D(N_D-1)}]^T. \quad (6b)$$

FIR and IIR Filters

It is well-known that the finite impulse response (FIR) filter and the infinite impulse response (IIR) filter are the two common types of linear filters used in signal processing. As described in various signal processing textbooks (e.g. see Ch. 6 and 7 in [22]), the FIR filter is a non-recursive filter whose output samples only depend on the input data samples, and hence its impulse response has a finite duration. On the other hand, the IIR filter is a recursive filter whose output samples depend on both input data samples and past output, and correspondingly its impulse response carries on for an infinite time. For both types of filters, the filter order is essentially equivalent to the number of input samples that each filter output depends on. A higher filter order can yield a sharper transition band and a more uniform passband in the filter's steady-state frequency response, but it also brings about a lengthening of the filter's transient response. Note that, for a K^{th} -order IIR filter, its n^{th} output sample can be expressed as follows:

$$y(n) = -\sum_{k=1}^K c_k y(n-k) + \sum_{k=0}^K b_k x(n-k), \quad (7a)$$

where c_k and b_k are the respective weights of past output samples and input samples used in the filter, and they can be found using approaches like Butterworth and Chebyshev design methods. The output for FIR filters essentially has the same form as shown in (7a) except that all the weights of past output samples are set to zero (i.e. $c_k=0$). The input weights for FIR filters can be found using approaches such as the windowing method and the Parks-McClellan algorithm.

From a state-space perspective, the output of both FIR and IIR filters can be considered as a joint contribution from the filter's initial state and the input samples. In particular, as described by Bjaerum *et al.* [23], the filter output can be expressed in the following vector form:

$$\mathbf{y} = \mathbf{T}\mathbf{v}_{\text{init}} + \mathbf{S}\mathbf{x}, \quad (7b)$$

where \mathbf{v}_{init} is the initial filter state vector of length K (i.e. the filter order), while \mathbf{T} and \mathbf{S} are respectively the transient filter matrix (of size $N_D \times K$) and the steady-state filter matrix (of size $N_D \times N_D$) whose entries depend on the filter weights c_k and b_k shown in (7a). For FIR filters, the initial filter state vector only affects the filter output for a finite duration; however, for IIR filters, this vector has an effect on the filter output all the time since the filter's impulse response never vanishes. As such, the initial state vector should be defined in a way so that the filter's transient effects can be mitigated. Based on this notion, a few studies have considered the use of time-variant initialization approaches like step initialization and projection initialization [24][25]. Recently, Bjaerum *et al.* [23] have shown that projection initialization is more effective because it gives a stopband frequency response that looks the most similar to the steady-state response. This initialization approach, as

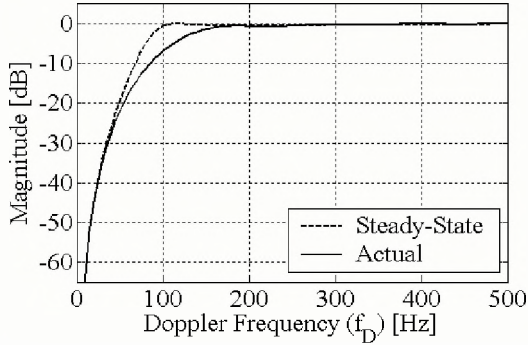


Figure 4. Actual and steady-state filter response of a projection-initialized IIR filter. Shown are the responses for a 3rd-order Chebyshev IIR filter (100 Hz nominal cutoff) when $N_D=10$. The Doppler sampling rate was 1 kHz.

originally proposed by Chornoboy [26], works by setting the initial state vector as the complement of the least-squares fitting coefficients between the transient filter matrix and the steady-state filter output. In particular, the initial state vector for projection initialization can be expressed as follows:

$$\mathbf{v}_{\text{init}} = -(\mathbf{T}^H \mathbf{T})^{-1} \mathbf{T}^H \mathbf{S} \mathbf{x} = -\mathbf{T}^+ \mathbf{S} \mathbf{x}, \quad (8a)$$

where the ‘+’ superscript denotes a pseudoinverse operation (i.e the singular matrix equivalent of a square matrix’s inverse). Correspondingly, by combining (5), (7b), and (8a), the overall filter matrix with projection initialization can be written as:

$$\mathbf{F} = [\mathbf{I} - \mathbf{T} \mathbf{T}^+] \mathbf{S}, \quad (8b)$$

where \mathbf{I} is an $N_D \times N_D$ identity matrix. Figure 4 shows an example of the frequency response for projection-initialized IIR filters. This figure was computed by substituting (8b) into (6a), and it shows that the actual response of the projection-initialized IIR filter is suboptimal, but close, to the steady-state filter response. Note that, besides the use of filter initialization schemes, minimum-phase filters can also be used to reduce transient filtering effects. For instance, Bjaerum *et al.* [23] have studied the use of minimum-phase FIR filters and have shown that they can improve the filtering performance.

Polynomial Regression Filters

Another method of suppressing clutter is to use a regression filter in place of FIR and IIR filters. This type of filter works by first modeling the clutter as a series of curve shapes and then computing the least-squares fitting residual between the Doppler signal and the given clutter model. From a subspace perspective, such regressive fitting is equivalent to a least-squares projection of the Doppler signal vector onto the orthogonal complement of the clutter model subspace. As described in various algebra textbooks (e.g. see Sec. 3.4.1 in [27]), the least-squares projection of a vector \mathbf{x} onto the orthogonal complement of a subspace matrix \mathbf{C} is given by:

$$\mathbf{y} = [\mathbf{I} - \mathbf{C}(\mathbf{C}^H \mathbf{C})^{-1} \mathbf{C}^H] \mathbf{x} = [\mathbf{I} - \mathbf{C} \mathbf{C}^+] \mathbf{x}. \quad (9a)$$

Correspondingly, the filter matrix for a regression filter can be expressed as follows:

$$\mathbf{F} = \mathbf{I} - \mathbf{C} \mathbf{C}^+. \quad (9b)$$

In terms of the curve shapes used for the clutter model, low-order polynomials are often suitable because clutter echoes are generally consisted of low frequency components. Thus, polynomial basis vectors are typically used for the columns of the clutter subspace matrix. For a K^{th} -order polynomial clutter model $\hat{\mathbf{c}}$, the subspace matrix \mathbf{C} is an $N_D \times (K+1)$ matrix that has the following form:

$$\hat{\mathbf{c}} = \sum_{k=0}^K \chi_k \mathbf{p}_k \Leftrightarrow \mathbf{C} = \begin{bmatrix} | & | & & | \\ \mathbf{p}_0 & \mathbf{p}_1 & \cdots & \mathbf{p}_K \\ | & | & & | \end{bmatrix}, \quad (10)$$

where χ_k and \mathbf{p}_k are the respective least-squares fitting coefficient and the length- N_D basis vector for the k^{th} -order polynomial (usually ranged between -1 and $+1$). Based on this notion, Hoeks *et al.* [28] have considered using first and second order polynomial clutter models, while Kadi and Loupas [25] have evaluated the use of polynomial models up to the fourth order. Torp [15] has subsequently generalized this filtering approach by using orthogonal polynomials such as Legendre or Chebyshev polynomials² for the clutter model. In terms of its performance, Bjaerum *et al.* [23] have shown that, for the same filter order, the polynomial regression filter have a similar frequency response as the one for the projection-initialized IIR filter at low nominal cutoff frequencies. However, the polynomial regression filter has lesser flexibility in adjusting the width of the filter stopband since the filter response can only be changed by varying the filter order (whereas IIR filters can also vary the nominal cutoff frequency). Note that, besides the use of polynomials, other basis sets such as wavelets can also be used for the regression filter. For instance, Cloutier *et al.* [29] have modeled clutter as a sum of Gabor wavelets (orthogonal bases with different frequencies and Gaussian envelopes) that match the principal Doppler signal contents.

4.2. Adaptive Filters

Background Considerations

When using non-adaptive filters for clutter suppression, it is inherently assumed that the clutter spectral contents of all the mapped pixels would fall within a certain low Doppler frequency band. As such, the same clutter filter is often applied to the Doppler signal of all map pixels. Nonetheless, clutter suppression would likely be more effective if the filter stopband can be selected adaptively according to the local clutter characteristics of individual map pixels. For instance, in performing clutter filtering on Doppler data acquired under substantial tissue motion, the filter stopband may need to be dynamically adjusted because the Doppler clutter of some map pixels may not be centered around zero frequency. Based on this principle, Yoo *et al.* [30] have proposed the use of a filter bank approach whereby the width of the filter stopband can be changed depending on the magnitude of the mean clutter

² Legendre and Chebyshev polynomials can be obtained by orthogonalizing the polynomial set $\{1, n, n^2, \dots\}$.

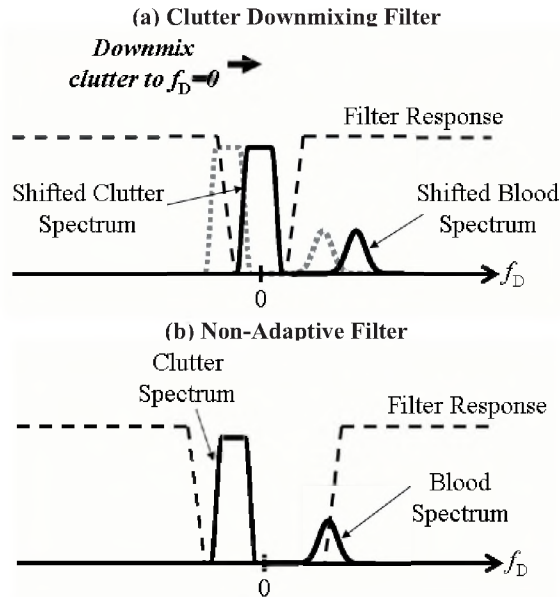


Figure 5. Illustration of the difference between (a) an adaptive filter based on clutter downmixing and (b) a non-adaptive clutter filter. For the non-adaptive filter, a wider stopband is needed to suppress clutter, but its use causes parts of the blood spectrum to be attenuated.

frequency. However, when a wider filter stopband is used, this clutter suppression approach may concomitantly suppress a substantial portion of the blood echoes in the Doppler spectrum, and as a result the sensitivity of flow detection may be decreased. In order to effectively suppress clutter originating from tissue motion, it is beneficial to design filters that can adapt its stopband to the clutter spectral characteristics. This rationale is the fundamental basis of adaptive clutter filters.

Clutter-Downmixing Filters

In the presence of tissue motion, one intuitive way of adaptively suppressing Doppler clutter is to design and use a bandpass filter whose stopband is centered at the mean clutter frequency. To implement this approach, however, high computation power would be required because of the need to design a different bandpass filter for each map pixel. As an equivalent way of realizing the same bandpass filter operation, it is possible to first downmix the Doppler signal with the mean clutter frequency before carrying out a highpass filtering operation. An illustration of this clutter downmixing strategy, which was originally introduced by Thomas and Hall [31] and Brands *et al.* [32], is shown in Figure 5. Mathematically, the n^{th} sample of the downmixed Doppler signal $x_{\text{DM}}(n)$ can be expressed as:

$$x_{\text{DM}}(n) = x(n)e^{-j\phi(n)} \quad \text{for } \phi(n) = 2\pi f_{\text{D}(c)} n T_{\text{PRI}}, \quad (11a)$$

where $\phi(n)$ is the instantaneous phase of the downmixing carrier, while $f_{\text{D}(c)}$ denotes the mean clutter frequency that can be estimated using closed-form estimators like the lag-one autocorrelator (to be described in Section 5). From a vector space perspective, the downmixing operation is equivalent to applying a diagonal matrix operator \mathbf{D} (of size

$N_{\text{D}} \times N_{\text{D}}$) to the Doppler signal vector \mathbf{x} . As such, the downmixed Doppler signal vector \mathbf{x}_{DM} can be written as:

$$\mathbf{x}_{\text{DM}} = \mathbf{D}\mathbf{x} \quad \text{for } \mathbf{D} = \text{diag}[e^{-j\phi(0)}, e^{-j\phi(1)}, \dots, e^{-j\phi(N_{\text{D}}-1)}]. \quad (11b)$$

After the downmixing, any type of non-adaptive filter can generally be used to suppress the zero-frequency centered Doppler clutter. Correspondingly, the overall filter matrix of a filter with clutter downmixing is simply equal to the multiplication between the original filter matrix \mathbf{F} and the downmixing operator \mathbf{D} . As seen in Figure 5, this filtering strategy is particularly useful when clutter and blood scatterers give Doppler frequency components of different signs (i.e. when they move in opposite directions), because in this case the blood spectrum can more likely be preserved after the downmixing step. Note that, as described by Bjaerum *et al.* [33], the performance of the downmixing filter can be further improved if instantaneous clutter frequencies are used for the phase terms in the downmixing operator. Nevertheless, to accurately estimate the instantaneous clutter frequencies, one would require the use of multiple Doppler signal vectors that are statistically stationary.

Eigen-Regression Filters

Another way of adaptively suppressing Doppler clutter is to directly analyze the composition of the Doppler signal and remove a composition subset that corresponds to clutter. This filtering strategy is essentially the same as using a regression filter whose clutter model consists of a subset of components seen in the Doppler signal composition. In terms of its implementation, the signal analysis can be effectively carried out by decomposing the Doppler data into a series of adaptable, orthogonal basis functions (as opposed to fixed ones like the Fourier expansion). As discussed in algebra textbooks (e.g. see Sec. 6.8 in [27]), such decomposition is often referred to as the Karhunen-Loeve (KL) expansion or principal component analysis, and it can be computed through eigen-decomposition of the Doppler signal's correlation matrix. For a Doppler ensemble size N_{D} , the KL expansion is given by:

$$\mathbf{x} = \sum_{k=1}^{N_{\text{D}}} \gamma_k \mathbf{e}_k \quad \text{for } E\{\gamma_k \gamma_l\} = \begin{cases} \lambda_k & , k = l \\ 0 & , k \neq l \end{cases}, \quad (12a)$$

where γ_k is the k^{th} expansion coefficient, while λ_k and \mathbf{e}_k are the respective eigenvalue and eigenvector corresponding to the k^{th} orthogonal basis function. Note that the eigenvalues and eigenvectors are related to the signal vector by:

$$\sum_{k=1}^{N_{\text{D}}} \lambda_k \mathbf{e}_k \mathbf{e}_k^{\text{H}} = E\{\mathbf{x}\mathbf{x}^{\text{H}}\} = \mathbf{R}_{\text{x}}, \quad (12b)$$

where $\mathbf{R}_{\text{x}} = E\{\mathbf{x}\mathbf{x}^{\text{H}}\}$ refers to the statistical correlation matrix of the Doppler signal. In practice, this matrix can be estimated via ensemble averaging as follows:

$$\mathbf{R}_{\text{x}} \approx \frac{1}{M} \sum_{m=1}^M \mathbf{x}_m \mathbf{x}_m^{\text{H}}, \quad (12c)$$

where M is the number of Doppler signal vectors (or snapshots) that are statistically stationary and \mathbf{x}_m indicates the Doppler signal vector for the m^{th} snapshot.

Since clutter often has a much higher strength than blood echoes and white noise, the signal decomposition

Table 1. Comparison of Existing Clutter Filter Designs

Type	Filter Equation	Stopband Adjustment	Advantage	Limitation
IIR + proj. initialization	$y = [I - TT^*]Sx$ (both T , S are fixed state-space matrices)	Through changes in filter order and nominal cutoff freq.	Simple to carry out once filter coefficients are found	Does not adapt to Doppler signal; efficacy depends on choice of filter parameters
Polynomial regression	$y = [I - CC^*]x$ (C is a fixed polynomial matrix)	By choice of clutter polynomial order	Same as above	Same as above
Clutter downmixing	$y = FDx$ (F is a fixed filter matrix; D is an adaptive downmixing matrix)	From changes to stopband of the non-adaptive filter	Improves highpass filtering by first downmixing clutter to zero frequency	Efficacy depends on choice of non-adaptive filter and accuracy of downmixing matrix
Eigen-regression	$y = [I - CC^*]x$ (C is an adaptive clutter subspace matrix)	Via selection of clutter eigen-space dimension	Adapts filter matrix to Doppler signal contents via KL expansion	Needs multiple snapshots to find correlation matrix; efficacy depends on choice of clutter dimension

given in (12a) would have high-energy basis functions (or principal components) that correspond to clutter. Hence, as pointed out by Bjaerum *et al.* [33], Doppler clutter can be suppressed by using the basis vectors of these high-energy components as the clutter model for a regression filter. In particular, when K of the N_D basis functions correspond to clutter (i.e. with a clutter eigen-space dimension equal to K), the resulting clutter model and the clutter subspace matrix for an eigen-based regression filter can be expressed as:

$$\hat{c} = \sum_{k=1}^K \lambda_k e_k \Leftrightarrow C = \begin{bmatrix} | & | & & | \\ e_1 & e_2 & \dots & e_K \\ | & | & & | \end{bmatrix}, \quad (13)$$

and the filter matrix would carry the same form shown in (10). Similar forms of this eigen-based filter have been reported in studies on swept-scan-based flow imaging [34] as well as strain-flow imaging [35]. Note that, as described by Ledoux *et al.* [36], the same filtering strategy can also be performed by applying singular value decomposition (SVD) to a multi-snapshot data matrix constructed from stacking together a number of stationary Doppler signal vectors. As well, as reported by Gallippi and Trahey [37], the Doppler spectral analysis can be carried out using another approach called independent component analysis that decomposes a signal into a series of statistically independent basis functions (as opposed to orthogonal ones). This latter approach has been applied to suppress clutter in acoustic radiation force imaging [38].

4.3. Comparison of Clutter Filters

Table I summarizes and compares the main features of the four types of clutter filters described in this section. From this table, it can be seen that the two non-adaptive filters (projection-initialized IIR and polynomial regression) are simpler to implement than adaptive filters because their filter matrix remains the same for a given set of filter parameters. However, the primary shortcoming of these non-adaptive filters is that they do not adapt to the Doppler signal contents. Because of this limitation, they inherently need a wider stopband to suppress Doppler clutter that has wideband characteristics and ones that are shifted away

from zero frequency. On another note, it is worth pointing out that amongst the two non-adaptive filters, the projection-initialized IIR filter seems to have more flexibility in defining the stopband since it can modify the filter response via changes in both the filter order and the nominal cutoff.

In contrast to the two non-adaptive filters, the clutter downmixing filter can be perceived as a partially adaptive filter. Specifically, its filter matrix is a joint product between a fixed matrix operator that makes use of non-adaptive filtering principles as well as an adaptive matrix operator that is intended to downmix the Doppler clutter to zero frequency. The advantage of this filtering approach is that the highpass filtering operation can likely be improved since the downmixed Doppler clutter is supposedly centered at zero frequency. Nevertheless, because of the hybrid nature of its filter matrix, the clutter downmixing filter's efficacy is inherently dependent on two factors: 1) the choice of the non-adaptive filter used for the fixed matrix operator, and 2) the accuracy of the downmixing matrix operator found by estimating the mean or instantaneous clutter frequencies of the Doppler data.

Amongst the four classes of filters considered, the eigen-regression filter seems to have the best adaptability to the Doppler signal contents. In particular, the filter matrix of this filter is defined adaptively according to the most principal basis vectors in the Doppler signal's KL expansion. In turn, the eigen-regression filter can more likely preserve non-clutter components of the Doppler signal unless they share the same principal basis vectors with clutter components. However, the formulation for this filter inherently requires the availability of Doppler data from multiple sample volumes with similar signal characteristics (i.e. statistically stationary). As such, this filter may be challenging to implement in some vascular imaging studies where it is difficult to segment out regions with similar Doppler data statistics. Another limitation of the eigen-regression filter is that its efficacy is rather sensitive to the choice of the clutter eigen-space dimension owing to the filter's adaptive nature. Hence, it is necessary to develop an effective algorithm for this filter to select the clutter eigen-space dimension.

5. EXISTING VELOCITY ESTIMATION METHODS

5.1. Non-Parametric Estimators

Background Considerations

As already pointed out, a two-stage process is often used to compute velocity estimates in color flow imaging. First, a clutter filter is applied to the Doppler signal of each sample volume to remove low-frequency echoes originating from tissues and vessel walls. The filtered signal is then passed into a non-parametric flow estimator to compute the mean flow velocity. For this two-stage estimation approach, it is presumed that the clutter filter can adequately suppress clutter so that the filtered Doppler data consists of just the blood echoes and filtered white noise. Based on this notion, the filtered Doppler data vector \mathbf{y} (of length N_D) can be described by the following signal model:

$$\mathbf{y} = [y(0), y(1), \dots, y(N_D - 1)]^T = \mathbf{b} + \mathbf{w}_f, \quad (14)$$

where $y(n)$ is the n^{th} filtered sample, while \mathbf{b} and \mathbf{w}_f respectively denote the signal vectors for blood echoes and filtered white noise. This signal model often serves as the starting point in the derivation of various non-parametric mean velocity estimators.

Frequency-Based Methods

One approach for finding the mean flow velocity is to first estimate the mean frequency of the filtered Doppler signal and then use the Doppler equation to convert the frequency estimate into a velocity value. In this estimation approach, the mean Doppler frequency can theoretically be computed by dividing between the first-order and zeroth-order Doppler spectral moments. Alternatively, by making use of the Wiener-Khinchin relation, the same computations can be carried out in a more efficient manner through an analysis of the Doppler autocorrelation function (i.e. without directly analyzing the Doppler spectrum). As first described by Kasai *et al.* [39] in the context of color flow imaging, the autocorrelation-based approach would lead to the following expression for the mean Doppler frequency:

$$f_{D(\text{est})} = \frac{\arg[R_y(1)]}{2\pi T_{\text{PRI}}} \quad \text{for } R_y(1) = \sum_{n=1}^{N_D-1} y(n)y^*(n-1), \quad (15)$$

where $R_y(1)$ is the Doppler autocorrelation function at a lag of one sample. Based on this equation, it can be seen that the lag-one autocorrelation phase is the primary factor in the mean Doppler frequency estimate. The phase quantity, however, is affected by signal aliasing due to the sampled nature of the Doppler data, and such a problem is often considered as a theoretical limitation of the autocorrelation estimator. Nevertheless, the aliasing limit is actually appreciated in practice because the unaliased velocity range is often used to define the mapping scale when designing the color map. Also, as pointed out by Tamura *et al.* [40], aliasing is sometimes introduced intentionally in color flow images to improve visualization of streamlines and laminar flow within the field of view.

The estimation variance of the lag-one autocorrelator given by (15) can be reduced by expanding the Doppler

autocorrelation into a two-dimensional (2D) function based on multiple Doppler signal snapshots within a given depth range [41]. However, its use in color flow data processing is often not vital because the estimation variance can also be reduced via spatial averaging of the velocity estimates from adjacent map pixels within the imaging view. As pointed out by Loupas *et al.* [42][43], another possible advantage of the 2D autocorrelation approach is that it can be used to jointly estimate both the mean Doppler frequency and the instantaneous carrier frequency. Such feature is useful for correcting the Doppler frequency biases originating from carrier frequency variations that arise when wideband pulses are used to acquire color flow data (even though this is not common in color flow imaging as noted in Section 3.2).

Time-Shift-Based Methods

Another approach for estimating the mean flow velocity is to find the average inter-pulse time shift between post-filter echo envelopes of the same beam line and then apply (1a) to convert the time shift estimate into a velocity value. As reviewed by Alam and Parker [44], this time-shift-based estimation approach is essentially derived from target track-ing principles that are used in radar and sonar. In terms of its implementation, time shift estimation can be performed in two different ways. The first way, as initially applied to color flow imaging by Bonnefous and Pesque [45], involves finding the average time lag that yields the maximum cross-correlation between successive echo envelopes of the beam line. The second way, as proposed by Ferrara and Algazi [46][47] as well as Alam and Parker [48], involves computing a time-shift likelihood function from geometric projection principles and then searching for its location of maximum. For both implementation approaches, their performance is not affected by carrier frequency variations because inter-pulse time shifts are not physically dependent on the carrier frequency (as seen in (1a)). They also do not suffer from aliasing problems since they are not based on the analysis of Doppler frequencies. However, the theoretical advantages offered by these estimators appear to be non-essential to color flow data processing (e.g. aliasing is indeed preferred in some flow studies as noted earlier). As such, time-shift estimators are often not used in color flow imaging, even though they have been a significant part of early research efforts in color flow signal processing.

5.2. Parametric Estimators

Background Considerations

In using non-parametric estimators to find flow velocities, estimation biases can be expected whenever the clutter filter distorts parts of the blood signal or fails to adequately suppress clutter. An illustration of this problem for a frequency-based non-parametric estimator is given in Figure 6a. Note that, at low blood-signal-to-noise ratios, further estimation biases can be anticipated because the filtered noise (i.e. colored noise) becomes a significant part of the filtered Doppler signal and in turn adds bias to the flow estimates. One of the ways to account for these clutter

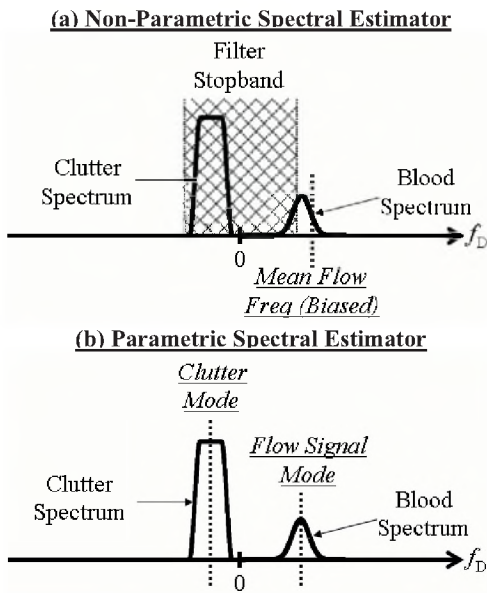


Figure 6. Difference between the spectral estimates of (a) non-parametric and (b) rank-two parametric flow estimators. Note that the mean estimate in (a) is biased away from the blood spectral peak because of filter distortions, while the two spectral modes in (b) are relatively unbiased.

filter biases is to apply a *post facto* correction factor to the flow estimates. For instance, Rajaonah *et al.* [49] have reported a frequency-based bias correction scheme that applies a correction factor based on the mean Doppler frequency of colored noise samples. Their approach, however, is intended to work with time-invariant clutter filters such as FIR filters, and thus it is not suitable for time-variant filters like projection-initialized IIR filters.

To effectively account for clutter filter biases, it is theoretically advantageous to use estimation strategies that can be directly applied to the raw Doppler signal. This rationale has motivated the development of parametric estimators that work by analyzing the principal Doppler spectral contents (i.e. they are frequency-based estimators). For these estimators, their principles are generally related to the following principal-component signal model:

$$\mathbf{x} = \mathbf{b} + \mathbf{c} + \mathbf{w} \approx \sum_{k=1}^K \chi_k \mathbf{v}_{\text{CS}(k)} + \mathbf{w} \quad (16a)$$

In the above expression, \mathbf{x} , \mathbf{b} , \mathbf{c} , and \mathbf{w} respectively denote the length- N_D vectors for raw Doppler signal, blood echoes, clutter, and white noise; also, K is the number of principal components in the signal model, while χ_k and $\mathbf{v}_{\text{CS}(k)}$ are the weight and complex sinusoid vector of the k^{th} component. Note that $\mathbf{v}_{\text{CS}(k)}$ essentially has the following vector form:

$$\mathbf{v}_{\text{CS}(k)} = [1, z_k, z_k^2, \dots, z_k^{(N_D-1)}]^T \quad \text{for } z_k = e^{j2\pi f_{D,k} T_{\text{PRI}}} \quad (16b)$$

where $f_{D,k}$ is the k^{th} principal Doppler frequency. It should be pointed out that, from a subspace perspective, this principal-component signal model is equivalent to the eigen-structure of a raw Doppler signal whose rank is equal to K . An illustration of the principal frequencies found using a rank-two parametric estimator is shown in Figure 6b.

Autoregressive Modeling

Autoregressive (AR) modeling (also known as linear prediction) is a type of parametric estimation approach that computes the principal Doppler frequencies through an all-pole signal analysis. As reviewed by Vaitkus and Cobbold [50] in the context of Doppler ultrasound, this approach begins by expressing each Doppler data sample as a linear combination of white noise and past data samples. In particular, for a K^{th} -order AR model, the n^{th} sample of the Doppler signal $x(n)$ is mathematically described by the following difference equation:

$$x(n) = w(n) - \sum_{k=1}^K c_k x(n-k), \quad (17a)$$

where $w(n)$ and c_k are respectively the white noise sample and the k^{th} model fitting coefficient. Correspondingly, this difference equation has the following all-pole form in the discrete frequency domain:

$$X_{\text{AR}}(f_D) = \frac{1}{1 + c_1 z^{-1} + \dots + c_K z^{-K}} \Big|_{z=e^{j2\pi f_D T_{\text{PRI}}}}, \quad (17b)$$

where z_k is the k^{th} characteristic mode (i.e. the k^{th} root of the denominator polynomial). From discrete-time signal theory, it is well-established that the difference equation's natural response takes on the same form as the principal-component signal model given in (16a) when no repeated modes are present. As such, the characteristic modes of the difference equation can be used to estimate the principal frequencies of the Doppler signal. Specifically, since z is defined as $\exp\{j2\pi f_D T_{\text{PRI}}\}$, the k^{th} principal Doppler frequency can be found from the k^{th} characteristic mode as follows:

$$f_{D,k} = \frac{\arg[z_k]}{2\pi T_{\text{PRI}}} \quad (18)$$

In turn, the modal flow frequency can be identified from the principal spectral estimate that has the largest magnitude:

$$f_{D(\text{est})} = f_{D,k_b} \quad \text{for } k_b = \arg \max_k \{ |f_{D,k}| \mid \forall k \in [1, K] \}. \quad (19)$$

In the AR model, the coefficients c_k in (17) are actually the main parameters that the characteristic modes depend on. These coefficients can be found by fitting the Doppler samples onto the data model. As discussed in spectral analysis textbooks (e.g. see Ch. 3 in [51]), an effective way of optimizing these coefficients is to minimize the mean-squared fitting error from both forward and backward regression perspectives. Such a least-squares fit can be computed using the Prony forward-backward fitting method (also known as modified covariance method). The forward-backward fitting procedure may be carried out recursively via an approach known as the Burg method.

In the context of color flow data processing, Loupas and McDicken [52] first considered the use of AR modeling in flow estimation. They showed that a first-order AR estimator, which only finds one Doppler spectral mode, is essentially equivalent to the lag-one autocorrelator shown in (15). Subsequently, Ahn and Park [53] attempted to use AR modeling in flow estimation studies that work with raw Doppler data. In particular, they developed a second-order AR estimator to simultaneously find the principal Doppler frequency of clutter and blood echoes. However, in this estimator, clutter is inherently assumed to be a single low-

frequency complex sinusoid. Such an assumption may not always be valid, especially in cases with wideband clutter.

Multiple Signal Classification

Another way of finding principal Doppler frequencies is to perform eigen-analysis on the correlation statistics of the Doppler signal. In particular, a form of eigen-analysis called multiple signal classification (MUSIC) has shown potential in obtaining flow estimates from the raw Doppler data. As applied to Doppler ultrasound by Allam and Greenleaf [54], the MUSIC method begins by decomposing the Doppler signal into a set of orthogonal bases through an eigen-decomposition of the Doppler correlation matrix (just like the eigen-regression filter as seen in (12)). Since the Doppler signal contents are mainly contained in the high-energy basis functions (due to their greater strength), the eigen-functions of the decomposition can then be divided into signal and noise components, thereby forming two mutually orthogonal subspaces. From this signal separation, a frequency pseudo-spectrum can subsequently be computed by finding the reciprocal of the cross-correlation between noise components and various complex sinusoids (with spectral peaks appearing at frequencies where the cross-correlation approaches zero). Specifically, for a Doppler signal with K principal components, its frequency pseudo-spectrum $X_{\text{MUSIC}}(f_D)$ can be expressed as:

$$X_{\text{MUSIC}}(f_D) = \frac{1}{\|\mathbf{E}_n^H \mathbf{v}_{\text{CS}}\|^2} = \frac{1}{\mathbf{v}_{\text{CS}}^H \mathbf{E}_n \mathbf{E}_n^H \mathbf{v}_{\text{CS}}}, \quad (20a)$$

where \mathbf{v}_{CS} is the complex sinusoid vector as seen in (6b) and \mathbf{E}_n is a noise subspace matrix consisting of the $N_D - K + 1$ least dominant eigenvectors:

$$\mathbf{E}_n = \begin{bmatrix} | & | & & | \\ \mathbf{e}_{K+1} & \mathbf{e}_{K+2} & \cdots & \mathbf{e}_{N_D} \\ | & | & & | \end{bmatrix}. \quad (20b)$$

As shown in spectral analysis textbooks (e.g. see Sec. 4.5 in [51]), the denominator in (20a) is a $(2N_D - 1)^{\text{th}}$ -order polynomial with K modes, and its polynomial coefficients are equal to the sum of elements along each diagonal of the matrix $\mathbf{E}_n \mathbf{E}_n^H$. Hence, like AR modeling, the eigen-modes in the MUSIC pseudo-spectrum can be found numerically by solving for the denominator roots, and correspondingly the modal flow frequency can be found from the principal frequency estimates using (18) and (19). Based on this root-finding principle, Vaitkus and Cobbold [55] developed a closed-form parametric estimator called Root-MUSIC to estimate principal flow velocities from raw Doppler data. Their approach, which uses a rank-two eigenstructure to model the raw Doppler signal, was analyzed using *in vivo* Doppler data whose clutter can be sufficiently modeled as a single complex sinusoid [56]. Note that another way to solve for the MUSIC eigen-modes is to use a peak searching algorithm to find the principal peaks in the pseudo-spectrum. Such an approach was used by Allam *et al.* [57] to process Doppler data acquired from a string phantom and a reflective surface that respectively simulate blood flow and stationary clutter.

Table 2. Comparison of Existing Frequency-Based Velocity Estimators

Type	Advantage	Limitation
Lag-one autocorrelator	Simple to implement with low computation demand	Only works on filtered Doppler data; prone to biases from filter distortions
AR estimator	Finds flow velocity directly from raw Doppler data without clutter filtering	Least-squares fit of c_k fails at high white noise levels; efficacy depends on choice of model order
MUSIC	Same as AR estimator, but more resilient to white noise	Needs multiple data snapshots to find correlation matrix; efficacy depends on eigen-structure rank

5.3. Comparison of Velocity Estimators

Like the comparison on clutter filter designs, Table 2 summarizes the advantages and limitations of the three frequency-based velocity estimators covered in this section. As indicated, the lag-one autocorrelator has the advantage of being computationally efficient. Indeed, the low computing burden of this estimator is well appreciated in early research and developments because of processing power limitations. However, as already pointed out, the lag-one autocorrelator can only be applied to filtered Doppler data, and thus, its velocity estimates are inherently prone to biases from clutter filter distortions.

Contrary to the lag-one autocorrelator, the AR estimator has the theoretical advantage of being able to obtain velocity estimates by directly processing the raw Doppler data. This estimator first uses a least-squares fitting procedure to compute the characteristic modes of the raw Doppler signal and then identifies the modal flow component based on the largest-frequency mode, thereby avoiding the need for clutter filtering. Nevertheless, the primary shortcoming of the AR estimator is that the least-squares fitting solution to the model coefficients assumes that the Doppler data samples are free of noise perturbations. Thus, its accuracy tends to degrade significantly as the noise level increases. Another limitation with the AR estimator is that its flow estimation performance is dependent on the choice of the model order (or eigen-structure rank). Specifically, a wrong choice of model order would give rise to spurious spectral modes and in turn give incorrect modal velocity estimates.

Unlike the AR estimator, the MUSIC estimator is more resilient to white noise because it first makes use of an eigen-decomposition procedure to separate the signal bases from noise floor components. Therefore, when applied to raw Doppler data with high noise levels, this estimator can obtain modal velocity estimates that are less biased than the ones found from AR modeling. On the other hand, it is worth pointing out that the formulation of MUSIC begins with the same eigen-decomposition step as seen for the eigen-regression filter. As such, MUSIC has a limitation

that is similar to the eigen-regression filter: it needs multiple signal snapshots that are statistically stationary in order to form an accurate estimate of the Doppler correlation matrix. Another limitation of the MUSIC approach is that, as similar to AR modeling, the performance of this estimator is contingent upon suitable choice of the eigen-structure rank. Thus, an adaptive rank selection algorithm is needed in order for this estimator to be effective in general.

6. CONCLUDING REMARKS

As seen in the previous two sections, eigen-based signal processing strategies have been the focus of the most recent research efforts in color flow data processing. In particular, both the eigen-regression filter and the MUSIC estimator have shown better potential than other signal processing methods in adapting to the Doppler signal characteristics. As such, eigen-based strategies seem to be more capable of obtaining flow estimates that are less affected by the signal processing error sources mentioned earlier in this article.

In terms of latest developments, a number of current research studies have been devoted to address the practical challenges of using eigen-based signal processing strategies. For instance, Lovstakken *et al.* [58] have recently studied the computational aspect of eigen-regression filters and have considered how the clutter eigen-space dimension can be adaptively selected based on the eigenvalue gradient in the KL expansion. They are also pursuing the development of a maximum-likelihood estimator that makes use of principal component analysis concepts [59]. Complementary to these studies, we have recently reported a new eigen-based clutter filter that works with single snapshots of Doppler data via the notion of principal Hankel component analysis [60]. As well, we have proposed a new eigen-based parametric estimator called the Matrix Pencil that treats velocity estimation as a generalized eigenvalue problem [61]. We have also developed an adaptive rank selection algorithm that is based on the spectral spread of the principal Doppler frequencies [62].

ACKNOWLEDGEMENTS

We are very grateful for Aziza Manceur's help on the French version of our abstract. We also wish to thank Larry Mo and ZONARE Medical Systems for supplying us with clinical flow images from their scanners.

This work was supported in part by grants from the Canadian Institutes of Health Research and the Natural Sciences and Engineering Research Council of Canada.

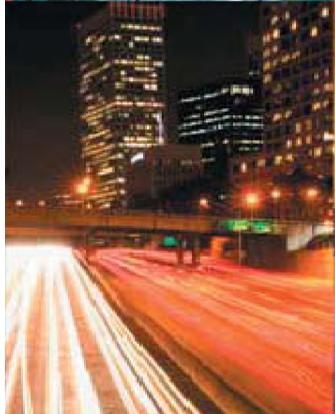
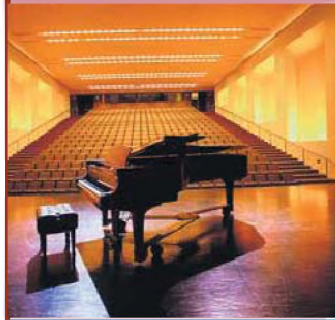
REFERENCES

- [1] K Ferrara and G DeAngelis, "Color flow mapping", *Ultrasound Med. Biol.*, vol. 23, pp. 321-345, 1997.
- [2] TH Williamson and A Harris, "Color Doppler ultrasound imaging of the eye and orbit", *Surv. Ophthalmol.*, vol. 40, pp. 255-267, 1996.
- [3] R Lagalla, G Caruso, and M Finazzo, "Monitoring treatment response with color and power Doppler", *Euro. J. Radiology*, vol. 28, pp. S149-S156, 1998.
- [4] AD Waggoner and SM Bierig, "Tissue Doppler imaging: a useful echocardiographic method for the cardiac sonographer to assess systolic and diastolic ventricular function", *J. Am. Soc. Echocardiogr.*, vol. 14, pp. 1143-1152, 2001.
- [5] G Armstrong, L Cardon, D Vilkomerson, *et al.*, "Localization of needle tip with color Doppler during pericardiocentesis: in vitro validation and initial clinical application", *J. Am. Soc. Echocardiogr.*, vol. 14, pp. 29-37, 2001.
- [6] KW Beach, AC Keith, JF Primozich, *et al.*, "Ultrasonic color flow mapping: the visualization of four-dimensional cardiac and vascular flow phenomena using two dimensions and real-time", *Ultrasound Med. Biol.*, vol. 23, pp. 347-363, 1997.
- [7] P Arbeille, MH Bouin-Pineau, and S Heralut, "Accuracy of the main Doppler methods for evaluating the degree of carotid stenosis (continuous wave, pulsed wave, and color Doppler)", *Ultrasound Med. Biol.*, vol. 25, pp. 65-73, 1999.
- [8] SFC Stewart, "Effects of transducer, velocity, Doppler angle, and instrument settings on the accuracy of color Doppler ultrasound", *Ultrasound Med. Biol.*, vol. 27, pp. 551-564, 2001.
- [9] A Fenster, DB Downey, and HN Cardinal, "Three-dimensional ultrasound imaging", *Physics Med. Biol.*, vol. 46, pp. R66-R99, 2001.
- [10] B Dunmire, KW Beach, KH Labs, *et al.*, "Cross-beam vector Doppler ultrasound for angle-independent velocity measurements", *Ultrasound Med. Biol.*, vol. 26, pp. 1213-1235, 2000.
- [11] SG Foster, CJ Pavlin, KA Harasiewicz, *et al.*, "Advances in ultrasound biomicroscopy", *Ultrasound Med. Biol.*, vol. 26, pp. 1-27, 2000.
- [12] PJA Frinking, A Bouakaz, J Kirkhorn, *et al.*, "Ultrasound contrast imaging: current and new potential methods", *Ultrasound Med. Biol.*, vol. 26, pp. 965-975, 2000.
- [13] RSC Cobbold, *Foundations of Biomedical Ultrasound*. New York City, USA: Oxford University Press, 2006.
- [14] DH Evans and WN McDicken, *Doppler Ultrasound: Physics, Instrumentation and Signal Processing*. 2nd Ed. West Sussex, UK: John Wiley & Sons Ltd., 2000.
- [15] H Torp, "Clutter rejection filters in color flow imaging: a theoretical approach", *IEEE Trans. Ultrason. Ferroelec. Freq. Contr.*, vol. 44, pp. 417-424, 1997.
- [16] A Heimdal and H Torp, "Ultrasound Doppler measurements of low velocity blood flow: limitations due to clutter signals from vibrating muscles", *IEEE Trans. Ultrason. Ferroelec. Freq. Contr.*, vol. 44, pp. 873-881, 1997.
- [17] KW Ferrara, VR Algazi, and J Liu, "The effect of frequency dependent scattering and attenuation on the estimation of blood velocity using ultrasound", *IEEE Trans. Ultrason. Ferroelec. Freq. Contr.*, vol. 39, pp. 754-767, 1992.
- [18] WH Round and RHT Bates, "Modification of spectra of pulses from ultrasonic transducers by scatterers in non-attenuating and attenuating media", *Ultrason. Imaging*, vol. 9, pp. 18-28, 1987.
- [19] PM Embree and WD O'Brien Jr, "Pulsed Doppler accuracy assessment due to frequency-dependent attenuation and Rayleigh scattering error sources", *IEEE Trans. Biomed. Eng.*, vol. 37, pp. 322-326, 1990.
- [20] JC Willemetz, A Nowicki, JJ Meister, *et al.*, "Bias and variance in the estimate of the Doppler frequency induced by a wall motion filter", *Ultrason. Imaging*, vol. 11, pp. 215-225, 1989.
- [21] C Tysoe and DH Evans, "Bias in mean frequency estimation of Doppler signals due to wall clutter filters", *Ultrasound Med. Biol.*, vol. 21, pp. 671-677, 1995.
- [22] AV Oppenheim, RW Schaffer, and JR Buck, *Discrete-time signal processing*. 2nd Ed. Upper Saddle River, USA: Prentice-Hall Inc., 1999.
- [23] S Bjaerum, H Torp, and K Kristoffersen, "Clutter filter design for ultrasound color flow imaging", *IEEE Trans. Ultrason. Ferroelec. Freq. Contr.*, vol. 49, pp. 204-216, 2002.
- [24] RB Peterson, LE Atlas, and KW Beach, "A comparison of IIR initialization techniques for improved color Doppler wall filter performance", *Proc. IEEE Ultrason. Symp.*, pp. 1705-1708, 1994.

- [25] AP Kadi and T Loupas, "On the performance of regression and step-initialized IIR clutter filters for color Doppler systems in diagnostic medical ultrasound", *IEEE Trans. Ultrason. Ferroelec. Freq. Contr.*, vol. 42, pp. 927-937, 1995.
- [26] ES Chornoboy, "Initialization for improved IIR filter performance", *IEEE Trans. Signal Processing*, vol. 40, pp. 543-550, 1992.
- [27] TK Moon and WC Stirling, *Mathematical methods and algorithms for signal processing*. Upper Saddle River, USA: Prentice-Hall Inc., 2000.
- [28] APG Hoeks, JJW van de Vorst, A Dabekaussen, *et al.*, "An efficient algorithm to remove low frequency Doppler signals in digital Doppler systems", *Ultrason. Imaging*, vol. 13, pp. 135-144, 1991.
- [29] G Cloutier, D Chen, and LG Durand, "A new clutter rejection algorithm for Doppler ultrasound", *IEEE Trans. Med. Imag.*, vol. 22, pp. 530-538, 2003.
- [30] YM Yoo, R Managuli, and Y Kim, "Adaptive clutter filtering for ultrasound color flow imaging", *Ultrasound Med. Biol.*, vol. 29, pp. 1311-1320, 2003.
- [31] L Thomas and A Hall, "An improved wall filter for flow imaging of low velocity flow", *Proc. IEEE Ultrason. Symp.*, pp. 1701-1704, 1994.
- [32] PJ Brands, APG Hoeks, and RS Reneman, "The effect of echo suppression on the mean velocity estimation range of the RF cross-correlation model estimator", *Ultrasound Med. Biol.*, vol. 21, pp. 945-959, 1995.
- [33] S Bjaerum, H Torp, and K Kristoffersen, "Clutter filters adapted to tissue motion in ultrasound color flow imaging", *IEEE Trans. Ultrason. Ferroelec. Freq. Contr.*, vol. 49, pp. 693-704, 2002.
- [34] DE Kruse and KW Ferrara, "A new high resolution color flow system using an eigendecomposition-based adaptive filter for clutter rejection", *IEEE Trans. Ultrason. Ferroelec. Freq. Contr.*, vol. 49, pp. 1384-1399, 2002.
- [35] C Kargel, G Hobenreich, B Trummer, and MF Insana, "Adaptive clutter rejection filtering in ultrasonic strain-flow imaging", *IEEE Trans. Ultrason. Ferroelec. Freq. Contr.*, vol. 50, pp. 824-835, 2003.
- [36] LAF Ledoux, PJ Brands, and APG Hoeks, "Reduction of the clutter component in Doppler ultrasound signals based on singular value decomposition: a simulation study", *Ultrason. Imaging*, vol. 19, pp. 1-18, 1997.
- [37] CM Gallippi and GE Trahey, "Adaptive clutter filtering via blind source separation for two-dimensional ultrasonic blood velocity measurement", *Ultrason. Imaging*, vol. 24, pp. 193-214, 2002.
- [38] CM Gallippi, KR Nightingale, and GE Trahey, "BSS-based filtering of physiological and ARFI-induced tissue and blood motion", *Ultrasound Med. Biol.*, vol. 29, pp. 1583-1592, 2003.
- [39] C Kasai, K Namekawa, A Koyano, and R Omoto, "Real-time two-dimensional blood flow imaging using an autocorrelation technique", *IEEE Trans. Sonics Ultrason.*, vol. 32, pp. 458-464, 1985.
- [40] T Tamura, RSC Cobbold, and KW Johnston, "Quantitative study of steady flow using color Doppler ultrasound", *Ultrasound Med. Biol.*, vol. 17, pp. 595-605, 1991.
- [41] H Torp, K Kristoffersen, and BAJ Angelson, "Autocorrelation techniques in color flow imaging: signal model and statistical properties of the autocorrelation estimates", *IEEE Trans. Ultrason. Ferroelec. Freq. Contr.*, vol. 41, pp. 604-612, 1994.
- [42] T Loupas, JT Powers, and RW Gill, "An axial velocity estimator for ultrasound blood flow imaging, based on a full evaluation of the Doppler equation by means of a two-dimensional autocorrelation approach", *IEEE Trans. Ultrason. Ferroelec. Freq. Contr.*, vol. 42, pp. 672-688, 1995.
- [43] T Loupas, RB Peterson, and RW Gill, "Experimental evaluation of velocity and power estimation for ultrasound blood flow imaging, by means of a two-dimensional autocorrelation approach", *IEEE Trans. Ultrason. Ferroelec. Freq. Contr.*, vol. 42, pp. 689-699, 1995.
- [44] SK Alam and KJ Parker, "Implementation issues in ultrasonic flow imaging", *Ultrasound Med. Biol.*, vol. 29, pp. 517-528, 2003.
- [45] O Bonnefous and P Pesque, "Time domain formulation of pulsed-Doppler ultrasound and blood velocity estimation by cross correlation", *Ultrason. Imaging*, vol. 8, pp. 73-85, 1986.
- [46] KW Ferrara and VR Algazi, "A new wideband spread target maximum likelihood estimator for blood velocity estimation—part I: theory", *IEEE Trans. Ultrason. Ferroelec. Freq. Contr.*, vol. 38, pp. 1-16, 1991.
- [47] KW Ferrara and VR Algazi, "A new wideband spread target maximum likelihood estimator for blood velocity estimation—part II: evaluation of estimators with experimental data", *IEEE Trans. Ultrason. Ferroelec. Freq. Contr.*, vol. 38, pp. 17-26, 1991.
- [48] SK Alam and KJ Parker, "The butterfly search technique for estimation of blood velocity", *Ultrasound Med. Biol.*, vol. 21, pp. 657-670, 1995.
- [49] JC Rajaonah, B Dousse, and JJ Meister, "Compensation of the bias caused by the wall filter on the mean Doppler frequency", *IEEE Trans. Ultrason. Ferroelec. Freq. Contr.*, vol. 41, pp. 812-819, 1994.
- [50] PJ Vaitkus and RSC Cobbold, "A comparative study and assessment of Doppler ultrasound spectral estimation techniques. Part I: estimation methods", *Ultrasound Med. Biol.*, vol. 14, pp. 661-672, 1988.
- [51] P Stoica and RL Moses, *Introduction to spectral analysis*. Upper Saddle River, USA: Prentice Hall Inc., 1997.
- [52] T Loupas and WN McDicken, "Low-order complex AR models for mean and maximum frequency estimation in the context of Doppler color flow mapping", *IEEE Trans. Ultrason. Ferroelec. Freq. Contr.*, vol. 37, pp. 590-601, 1990.
- [53] YB Ahn and SB Park, "Estimation of mean frequency and variance of ultrasonic Doppler signal by using second-order autoregressive model", *IEEE Trans. Ultrason. Ferroelec. Freq. Contr.*, vol. 38, pp. 172-182, 1991.
- [54] ME Allam and JF Greenleaf, "Isomorphism between pulsed-wave Doppler ultrasound and direction-of-arrival estimation—Part I: basic principles", *IEEE Trans. Ultrason. Ferroelec. Freq. Contr.*, vol. 43, pp. 911-922, 1996.
- [55] PJ Vaitkus and RSC Cobbold, "A new time-domain narrowband velocity estimation technique for Doppler ultrasound flow imaging. Part I: theory", *IEEE Trans. Ultrason. Ferroelec. Freq. Contr.*, vol. 45, pp. 939-954, 1998.
- [56] PJ Vaitkus, RSC Cobbold, and KW Johnston, "A new time-domain narrowband velocity estimation technique for Doppler ultrasound flow imaging Part II: comparative performance assessment", *IEEE Trans. Ultrason. Ferroelec. Freq. Contr.*, vol. 45, pp. 955-971, 1998.
- [57] ME Allam, RR Kinnick, and JF Greenleaf, "Isomorphism between pulsed-wave Doppler ultrasound and direction-of-arrival estimation—Part II: experimental results", *IEEE Trans. Ultrason. Ferroelec. Freq. Contr.*, vol. 43, pp. 923-935, 1996.
- [58] L Lovstakken, S Bjaerum, K Kristoffersen, *et al.*, "Real-time adaptive clutter rejection filtering in color flow imaging using power method iterations", *IEEE Trans. Ultrason. Ferroelec. Freq. Contr.*, vol. 53, pp. 1597-1608, 2006.
- [59] L Lovstakken, TA Tangen, S Bjaerum, and H Torp, "Optimum velocity estimation in ultrasound color flow imaging in presence of clutter noise", *Proc. IEEE Ultrason. Symp.*, pp. 2417-2420, 2006.
- [60] ACH Yu and RSC Cobbold, "A new eigen-based clutter filter using the Hankel-SVD approach", *Proc. IEEE Ultrason. Symp.*, pp. 1079-1082, 2006.
- [61] ACH Yu, LYL Mo, RK Warriner, and RSC Cobbold, "A new eigen-based flow estimator using the Matrix Pencil approach", *Proc. IEEE Ultrason. Symp.*, pp. 1335-1338, 2005.
- [62] ACH Yu and RSC Cobbold, "A Matrix Pencil estimator with adaptive rank selection: application to *in vivo* flow studies", *Proc. IEEE Ultrason. Symp.*, pp. 2015-2018, 2006.

831 sound level meter/real time analyzer

- Consulting engineers
- Environmental noise monitoring
- Highway & plant perimeter noise
- Aircraft noise
- General Surveys
- Community noise



FEATURES

- Class 1/Type 1 sound level meter
- Small size with large display. Ergonomic
- User friendly operator interface
- 120MB standard memory expandable up to 2GB
- Single measurement range from 20 to 140 dB SPL
- Up to 16 hours of battery life
- Provided with utility software for instrument set-up and data download
- Field upgradeable
- AUX port for connection to USB mass storage & cellular modems



MEASUREMENT CAPABILITIES

- Real time 1/1 & 1/3 octave frequency analysis
- Simultaneous display of several noise measurements—ANY DATA (Leq, Lmax, Spectra, etc)
- Automatic logging of user selectable noise measurements (Leq, Lmax, Spectra, etc...)
- Exceedance logging with user selectable trigger levels
- Audio and voice recording with replay

